# Green Synthesis and Characterization of a Hydrazone-Based Copper Complex with Antibacterial Activity: Experimental and DFT Studies

Husna Syaima[1], Sentot Budi Rahardjo[2,*], Yusica Amalia Rasyda[3], Soerya Dewi Marliyana[2], Agung Prakoso[3]

[1]Department of Chemistry, Faculty of Mathematics and Natural Sciences, Mulawarman University, Jl. Barong Tongkok, Gunung Kelua, Samarinda, 75123, Indonesia
[2]Department of Chemistry, Faculty of Mathematics and Natural Sciences, Sebelas Maret University, Jl. Ir. Sutami No.36A, Surakarta, 57126, Indonesia
[3]Chemistry Graduate Program, Faculty of Mathematics and Natural Sciences, Sebelas Maret University, Jl. Ir. Sutami No.36A, Surakarta, 57126, Indonesia

*Author to whom correspondence should be addressed:
E-mail: sentotbr@staff.uns.ac.id

(Received November 07, 2024; Revised September 30, 2025; Accepted April 21, 2026)

**Abstract**: This research focused on the green synthesis, experimental and computational structure analysis, and investigation of the antibacterial properties of a copper complex with Schiff base ligand, (Z)-2-(1-(2-phenylhydrazineylidene)ethyl)phenol. The ligand was synthesized from phenylhydrazine and o-hydroxyacetophenone with an acetic acid catalyst. The Cu(II) complex was synthesized by reacting $CuSO_4 \cdot 5H_2O$ with the ligand in methanol, using mole ratios of 1:4 and 1:1 with the addition of KOH at room temperature. The ligand was coordinated to Cu(II) via N-H and O-H groups. Electronic spectra at 643 nm suggested square planar geometry. The complex demonstrated higher antibacterial activity than most tested bacteria.

**Keywords:** antibacterial; copper complex; phenylhydrazine; Schiff base

## 1. Introduction

Metals in complex compounds confer several advantages regarding their biological activities, enhancing the efficacy of both ligands and metal ions[1)]. However, not all metal ions are suitable for synthesizing these compounds, making the selection of the appropriate metal a critical factor in determining their biological activity. Transition metals, commonly used to synthesize complex compounds, exhibit various biological activities[2)]. Frequently studied 3d metal ions include Zn(II), Cd(II), Cu(II), Co(II), and Ni(II)[2,3)]. Among these, 3d transition metal complexes are particularly advantageous due to their lower toxicity and higher cell membrane penetration compared to 4d and 5d series metals[4)].

Copper (Cu), particularly Cu(II), is extensively utilized in the synthesis of complex compounds for various applications due to its superior stability compared to other transition metals, such as iron (Fe) and cobalt (Co). Copper also functions as a trace element in the human body[5)]. Cu(II) complexes, in particular, exhibit superior biological activities. Previous research has demonstrated that Cu(II) complexes exhibit significantly greater antibacterial activity when compared to Co(II) and Ni(II) complexes[6)]. Cu(II) complexes have also shown higher antimicrobial activities than other metal complexes against various bacteria and fungi[7,8)]. The biological activity of Cu(II) complexes is primarily due to the release of $Cu^{2+}$ ions and the subsequent generation of reactive oxygen species (ROS). These ROS, particularly toxic hydroxyl radicals, can cause significant oxidative stress, leading to the disruption of microbial cell membranes. This damage compromises the integrity of the cells, making it difficult for them to maintain essential functions, ultimately resulting in the death of the microorganism. Additionally, the copper ions may interfere with key metabolic processes, further enhancing the antimicrobial effect of Cu(II) complexes[9,10)].

The choice of ligand plays a pivotal role in synthesizing biologically active complex compounds. Schiff-base ligands have garnered considerable attention due to their ease of synthesis from readily available starting materials, along with their diverse pharmacological activities[11,12)]. Schiff base ligands can coordinate to metals, enhancing their biological properties due to additional donor atoms[13)].

Cite: H. Syaima et al., "Green Synthesis and Characterization of a Hydrazone-Based Copper Complex with Antibacterial Activity: Experimental and DFT Studies". Evergreen, 13 (02) 863-875 (2026). https://doi.org/10.5109/7434179.

The azomethine group (C=N) in Schiff bases is associated with various biological activities, including antibacterial, antifungal, herbicidal, and other clinical applications[14]. Thus, Schiff base complexes are promising candidates as biologically active agents[15].

Hydrazones, a class of Schiff bases, are formed from the reaction of hydrazine (with a primary amine group) and aldehydes or ketones. These compounds can contain various heteroatoms in their structures, making them versatile multidentate ligands in coordination chemistry, facilitating chelation and diverse applications[16]. Hydrazone and its derivatives are being increasingly explored in pharmaceutical research due to their excellent biological activities[17]. Metal-based antimicrobial complexes derived from hydrazone Schiff bases have shown promising results against various bacterial and fungal pathogens[18].

Given these promising findings, Cu(II) complexes with Schiff base derivatives of hydrazone, particularly those derived from phenylhydrazine and ortho-hydroxyacetophenone, present a high potential for development as new bioactive compounds, especially as a novel antibacterial agent. The World Health Organization has emphasized the urgent need for new, effective antibacterial agents due to the rising resistance of bacteria to multiple antibiotics, which could lead to millions of deaths from hard-to-treat bacterial infections[19,20]. Some resistant strains (*Acinetobacter baumannii*, Carbapenem-resistant *Pseudomonas aeruginosa*, and Methicillin-resistant *Staphylococcus aureus, etc.)* exemplify the critical challenge posed by antibiotic resistance[21,22].

Herein, we report the synthesis of (Z)-2-(1-(2-phenylhydrazineylidene)ethyl)phenol (L), its coordination with Cu(II), and its antibacterial activities. The synthesis of L, from phenylhydrazine and o-hydroxyacetophenon as shown in Figure 1, and its complex was conducted at room temperature, yielding a facile, green, and efficient method for the synthesis of organic-inorganic materials. The antibacterial activity of Cu(II) with L against *Staphylococcus aureus*, *Staphylococcus epidermidis*, *Escherichia coli*, and *Pseudomonas aeruginosa* was also compared with that of the copper complex with a phenylhydrazine ligand synthesized in previous studies[23].

## 2. Experimental

### 2.1. Chemicals

The chemicals used in this research were obtained from Sigma-Aldrich and used as received, without any further purification.

### 2.2. Synthesis of (Z)-2-(1-(2-phenylhydrazineylidene)ethyl)phenol (L)

A solution of phenylhydrazine (0.683 g, 5 mmol) and o-hydroxyacetophenone (0.541 g, 5 mmol) was prepared by dissolving the two compounds in 3 mL of methanol, with the addition of three drops of glacial acetic acid. The mixture solution was stirred at room temperature for 1 hour, leading to the formation of a yellowish-white precipitate. Thin-layer chromatography (TLC) was used to monitor the reaction progress, employing a solvent system of n-hexane and ethyl acetate in a 9:1 ratio. Afterward, the precipitate was filtered, thoroughly washed with methanol and water, and then dried to obtain the final product.

### 2.3. Synthesis of Cu(II)-L Complex

The synthesis was based on Wang et al. (2019), with some modifications[24]. $CuSO_4 \cdot 5H_2O$ (0.249 grams; 1 mmol) was dissolved in 5 mL of methanol and then added dropwise to a solution of L (1 mmol; 0.226 grams) in 5 mL of methanol. The mixture was neutralized using a few drops of KOH (1 mmol) and stirred for 1 hour, resulting in a light brown precipitate. The solution was allowed to stand, and the precipitate formed was filtered, washed with methanol, and dried under a vacuum. Yield: 83.01%

### 2.4. Cu(II) Complex with Phenylhydrazine

The synthesis procedure and structural data of $[Cu(phenylhydrazine)_2(SO_4)] \cdot 5H_2O$ have been published in another publication.[23] Coordination structure of the complex is shown in Figure 2.

### 2.5. Instrumentation

A Lambda 25 Perkin Elmer spectrometer was used to analyze the electronic transitions and confirm the formation of the complex. The structural elucidation and purity of the synthesized compound were verified using an Agilent 500 MHz NMR spectrometer. The Shimadzu AA-

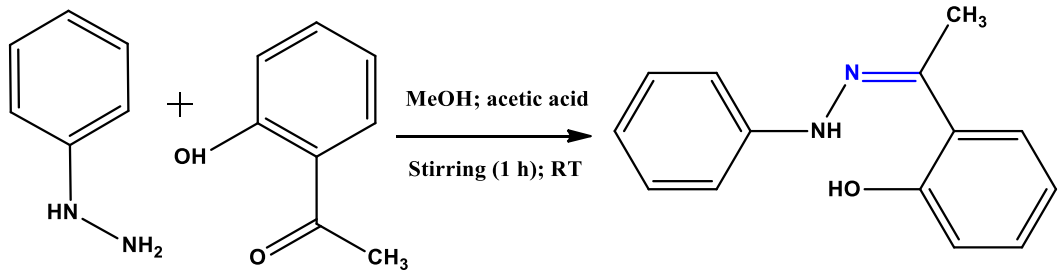


**Fig. 1:** Synthesis scheme of the Schiff base ligand (L)

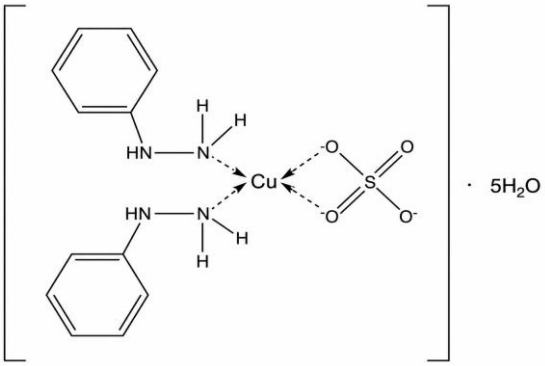


**Fig. 2:** Coordination structure of $[Cu(phenylhydrazine)_2(SO_4)]\cdot 5H_2O$

6650 Atomic Absorption Spectrophotometer (AAS) was used to determine the elemental composition and metal content, ensuring accurate quantification of metal ions within the complex. Thermal properties and stability were assessed using a TGA/DSC Diamond PerkinElmer in the 30-500 °C temperature range and a heating rate of 10 °C/min. Functional groups and bonding interactions were identified using FT-IR spectroscopy, performed on a Prestige-21 Shimadzu spectrophotometer. Magnetic properties were examined using a Magnetic Susceptibility Balance (Auto Sherwood Scientific 1016), offering valuable information on the metal center's magnetic behavior and oxidation state. Additionally, the Jenway CE 4071 Conductivity Meter was utilized to measure the electrical conductivity of the metal complex in solution. complex compounds and standard metal salts, namely $CuSO_4\cdot 5H_2O$, $FeSO_4\cdot 7H_2O$, $CuCl_2\cdot 2H_2O$, $NiCl_2\cdot 6H_2O$, $CoCl_2\cdot 6H_2O$, and $Fe(NO_3)_3\cdot 9H_2O$, were each dissolved in DMSO and prepared at the same concentration ($1.10^{-3}$ M).

## 2.6. Computational methods

Geometry optimization of all compounds was successfully performed using DFT calculations. The initial stages employed a split valence (SV) basis set, which was subsequently refined using the def2-SV(P) basis set with specified polarization on heavy elements. The HayWadt effective core potential (ECP) was applied to copper (Cu) and sulfur (S) atoms in final optimization step for enhanced computational efficiency. The optimization successfully converged under tight thresholds for both the geometry and the self-consistent field (SCF) leading to a well-converged structure. A crucial step in the workflow was the validation of the optimized geometry using a frequency analysis. The absence of imaginary frequencies was then confirmed with PBE0 model and def2-SV(P) basis set without ECP for better accuracy. This positive result verifies that the structure resides at a true minimum on the potential energy surface. The reliable calculation of excited-state properties proceeded with this validated ground-state structure using time-dependent DFT (TD-DFT) with PBE0 model, def2-TZVPD basis set for all atoms except H, for which the def2-SVPD basis set was used, and tight SCF convergence parameters. These DFT and TD-DFT calculations are simulated with implicit DMSO solvation using CPCM model and corrected with the D4 atom-pairwise dispersion correction. Main computational works are executed using ORCA 6.0.1 package. All results are visualized using Avogadro 1.2.0.

## 2.7. Media Preparation

Seventeen grams of Muller Hinton Agar (MHA) were dissolved in 500 mL of distilled water, then heated and stirred. The media was sterilized in an autoclave for 15 minutes, then transferred into test tubes, covered with cotton wool (a process conducted near a flame), and placed in an inclined position at room temperature for 24 hours.

## 2.8. Antibacterial Inhibition Test

The media agar was poured into Petri dishes and left to solidify. One inoculation loop of bacteria was dissolved in NaCl solution (9% in water). $CuSO_4\cdot 5H_2O$, L, phenylhydrazine, $[Cu(L)SO_4]$, and Cu(II)-phenylhydrazine were dissolved in DMSO solvent at varying concentrations of 250, 500, 1000, 2000, and 3000 µg/mL. A micropipette was used to apply 15 µL of each compound solution onto a paper disk, resulting in final concentrations of 3.75, 7.5, 15, 30, and 45 µg/disk. The bacterial suspension was spread evenly on the solid agar surface. Paper disks containing tested compounds were put on the media and incubated for 24 hours.

# 3. Results and Discussion

## 3.1. Synthesis of the Schiff Base Ligand

The synthesis of (Z)-2-(1-(2-phenylhydrazineylidene)ethyl)phenol (L) was based on a Schiff base reaction in which the ketone group on o-hydroxyacetophenone can react with the primary amine group on phenylhydrazine to form an imine or azomethine group (-C=N), accompanied by the release of water molecules (Figure 1).

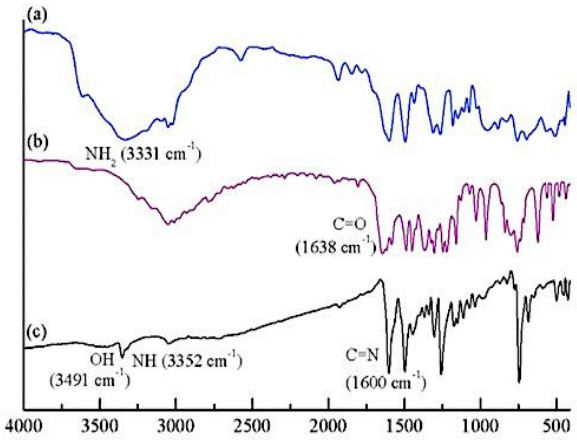


**Fig. 3:** Structure of the Schiff base ligand (L)

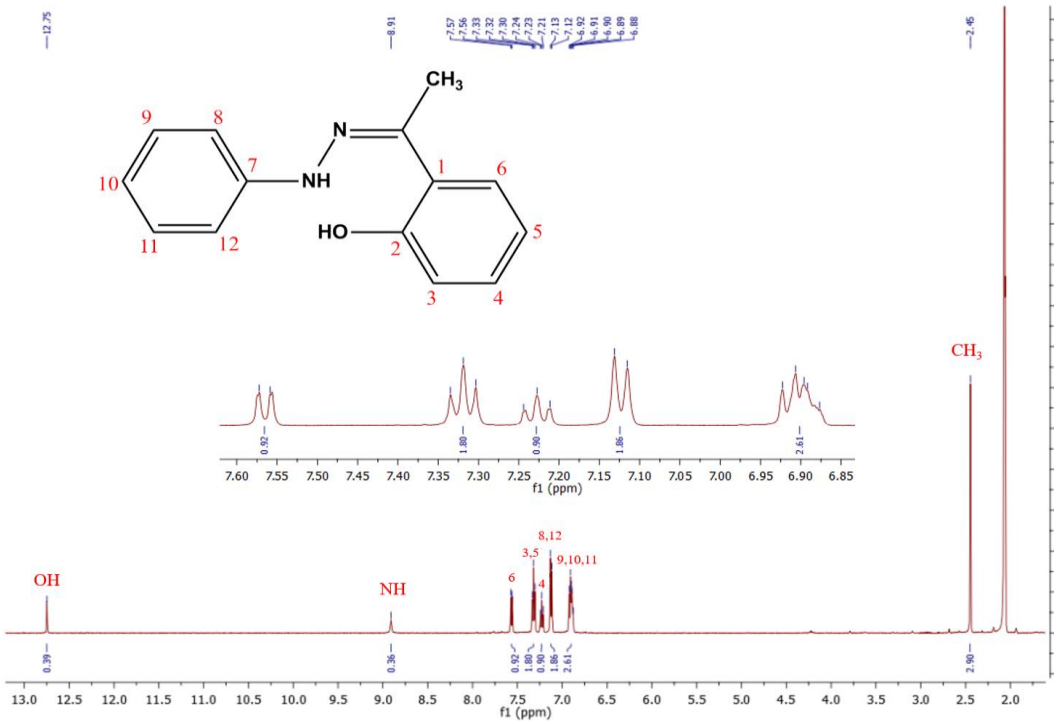


**Fig. 4:** $^{1}$H-NMR spectrum of L

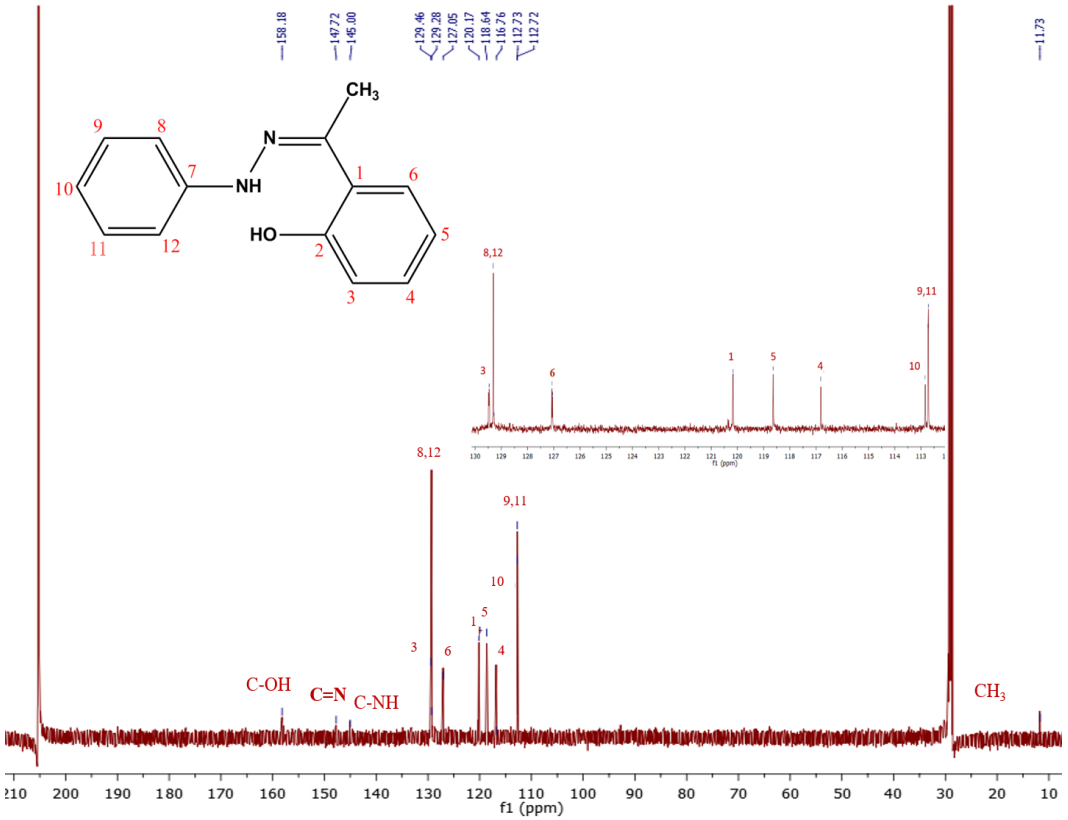


**Fig. 5:** $^{13}$C-NMR spectrum of L

The formation of the C=N group in a reaction depends on pH, where acidic conditions can accelerate the reaction. However, choosing the right acid catalysts is vital because too strong acids can cause amines to be protonated and become non-nucleophilic, making it difficult for them to attack the ketone compounds. The purity of the ligand product was analyzed using infrared spectroscopy, $^{1}$H NMR, and $^{13}$C NMR as presented in Figures 3-5.

Cite: H. Syaima et al., "Green Synthesis and Characterization of a Hydrazone-Based Copper Complex with Antibacterial Activity: Experimental and DFT Studies". Evergreen, 13 (02) 863-875 (2026). https://doi.org/10.5109/7434179.

## 3.2. Synthesis and Characterization of Cu(II)-L Complex

The synthesis of Cu(II) complex with L was carried out at room temperature. After adding $CuSO_4 \cdot 5H_2O$ solution to the L solution, precipitates were immediately formed. Several analyses, including AAS, TG-DSC, molar conductivity, infrared spectra, electronic spectra, and magnetism, that estimate the complex formula reinforced the indications of complex formation.

AAS was used to calculate the metal content in the compound. The estimated formula of the metal complex can be determined by comparing the experimental copper content in the complex with the theoretical content corresponding to the various possible complex formulas. The experimental total copper in the complex was 16.42%. Based on the comparison in Table 1, the possible formula of the Cu(II)-L complex is $Cu(L)SO_4(H_2O)_n$ (n=0, 1, and 2).

TGA analysis can reveal the thermal properties of the material[25] while DSC is for specific heat measurement[26]. It was also employed to characterize the number and position of water molecules in a complex, either as hydrates or ligands. The thermograms of the complex are presented in Figure 6**.** For the Cu(II)-L complex, the thermogram remains stable up to 200°C, indicating the absence of water molecules as hydrates or ligands. This stability suggests a complex formula of $Cu(L)SO_4$. The mass reduction begins at 201°C, with the presence of exothermic reactions, indicating the decomposition of organic compounds. Subsequently, an exothermic reaction occurred with a second mass decrease at 352 °C, and the mass decrease continued until 482 °C, which is also an indication of ligand decomposition. Formation of CuO residue is indicated above 500°C.

The conductivity of the complex was measured to evaluate its electrolytic behavior. The Cu(II)-L complex solution showed a molar conductivity value of 0 $S \cdot cm^2/mol$, as shown in Table 2, indicating it is neutral or non-electrolytic, with no charge from cations or anions present.

This implies there are no free counterions in the solution. Additionally, sulfate ions were found to be directly coordinated to the Cu(II). Therefore, the plausible formula of Cu(II)-L complex becomes $[Cu(L)SO_4]$.

FTIR analysis demonstrates the absorption of functional groups in the compounds[27]. The infrared spectra of the Schiff base ligand and the Cu(II) complex are shown in Figure 7. For the L, there is a shift in the absorption of OH (phenol) and secondary amine (-NH) groups from 3491 and 3352 $cm^{-1}$ to 3334 and 3181 $cm^{-1}$, respectively, in the $[Cu(L)SO_4]$ complex, suggesting coordination via these groups. The azomethine group (C=N) exhibits no indicating that it does not participate in coordination. New absorptions in the regions 1206, 1141, 1092, and 868 $cm^{-1}$ and 1230, 1122, 1041, and 863 $cm^{-1}$ correspond to sulfate groups ($-SO_4$), which coordinate with Cu(II) as a bidentate ligand. Furthermore, new absorptions below 500 $cm^{-1}$ indicate the presence of Cu-O and Cu-N bonds, confirming coordination in the complex. The Cu-O and Cu-N

**Table 1:** The copper content in Cu(II)-L complex

| Possible complex formula | Mr (g/mol) | Theoretical (%) | Experimental (%) |
|---|---|---|---|
| $Cu(L)SO_4$ | 385.50 | 16.47 | 16.42 ± 0.35 |
| $Cu(L)SO_4H_2O$ | 403.50 | 15.73 | |
| $Cu(L)SO_4(H_2O)_2$ | 421.50 | 15.06 | |

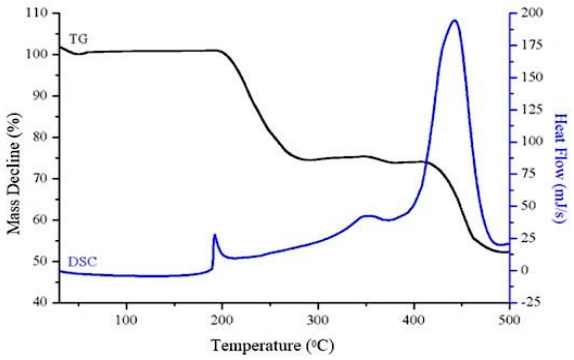


**Fig. 6:** TG-DSC thermogram of $[Cu(L)SO_4]$

**Table 2:** Molar conductivity of Cu(II)-L and some metal salts

| Compounds | Molar conductivity ($S.cm^2/mol$) | Ratio of cation and anion | Number of ions |
|---|---|---|---|
| DMSO | 0 | - | - |
| $CuSO_4 \cdot 5H_2O$ | 2 | 1:1 | 2 |
| $FeSO_4 \cdot 7H_2O$ | 2 | 1:1 | 2 |
| $CuCl_2 \cdot 2H_2O$ | 11 | 2:1 | 3 |
| $CoCl_2 \cdot 6H_2O$ | 21 | 2:1 | 3 |
| $NiCl_2 \cdot 6H_2O$ | 28 | 2:1 | 3 |
| $Fe(NO_3)_3 \cdot 9H_2O$ | 61 | 3:1 | 4 |
| $[Cu(L)SO_4]$ | 0 | - | - |

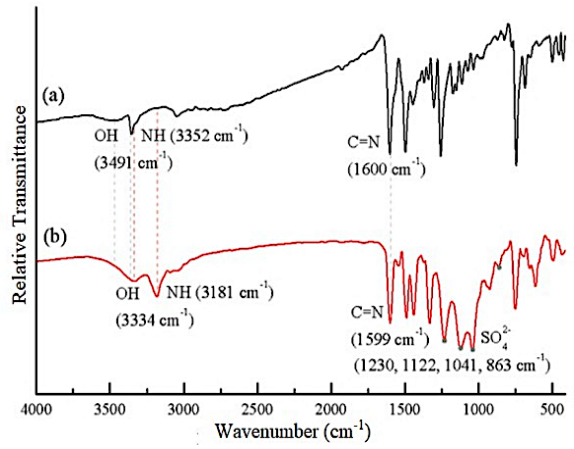


**Fig. 7:** Infrared absorption of L (a) and $[Cu(L)SO_4]$ (b)

absorptions appear at 492 and 434 $cm^{-1}$ in the Cu(II)-L complex.

UV-Vis spectrophotometry was used to analyze the corresponding absorbances.[28] Figure 8 depicts the electronic spectra of L and its complex, showing that the Maximum wavelength of $[Cu(L)SO_4]$ is 643 nm. The square planar complex exhibits a d-d transition peak below 700 nm, divided into three allowed transitions: $^2B_{1g}\rightarrow{}^2A_{1g}$, $^2B_{1g}\rightarrow{}^2B_{2g}$, and $^2B_{1g}\rightarrow{}^2E_g$[29]. Despite this, the electronic spectra display only one absorption peak resulting from the d-d transition due to the close energy levels of the three transitions, forming a single broad absorption peak[17,30]. Additionally, the complex shows absorption peaks above 14000 $cm^{-1}$ with a molar absorptivity exceeding 100 L/mol.cm[31,32]. Consequently, $[Cu(L)SO_4]$ is identified as a square planar complex. The compelling magnetic moment of $[Cu(L)SO_4]$ was 1.81 B.M., indicating paramagnetism with one unpaired electron[33]. This also suggests a flat rectangular geometry and a mononuclear complex, as they lack a Cu-Cu bond, resulting in a smaller magnetic moment of 1.73 B.M.[29,34]. Thus, the proposed structure of $[Cu(L)SO_4]$ is depicted in Figure 9.

## 3.3. DFT Calculation

The objective of this computational study is to reveal changes in electronic properties during the formation of ligands and Cu(II) complexes, as well as to explain the contribution of metal-ligands to their reactivity through HOMO-LUMO analysis and global reactivity parameters. In addition, this study aims to provide a theoretical basis that supports the enhancement of the antibacterial activity of complexes through an understanding of the mechanism of electron transfer and orbital stability.

Analysis of the molecular orbitals (Figure 10) shows that the formation process of Schiff base L and the Cu(II) complex gradually decreases the energy gap compared to the phenylhydrazine precursor. The HOMO refers to the energy level of the most highly filled molecular orbital, whereas the LUMO corresponds to the energy level of the lowest orbital that remains unoccupied[35]. In phenylhydrazine (Figure 10a), the HOMO is mainly delocalized on the -NH-NH- group and the phenyl ring, while the LUMO is located on the aromatic π system, with a relatively large HOMO-LUMO energy gap ($E_g$ = 5.71 eV). After condensation with o-hydroxyacetophenone, ligand L is formed (Figure 10b), the conjugated π system becomes longer, so that the LUMO level is stable (-1.04 eV) and the energy gap shrinks to 4.36 eV.

Furthermore, coordination to Cu(II) decreases the energy gap and alters the character of the electronic transition. In the $[Cu(phenylhydrazine)_2SO_4]$ complex (Figure 10c), the HOMO is centered on the Cu(II) atom and the N donor, while the LUMO is strongly localized on one phenylhydrazine ligand, resulting in $E_9$ = 3.53 eV, which indicates significant contributions from metal-to-ligand (MLCT) and intra-ligand (π→π*) transitions. The $[Cu(L)SO_4]$ complex (Figure 10d) has the smallest energy gap ($E_9$ = 3.30 eV). The HOMO is dominated by the phenolate-N(azomethine)-Cu orbital, while the LUMO is located on the π framework of the ligand, indicating a mixture of intra-ligand and ligand-to-metal (LMCT) character. The systematic decrease in energy gap from the free ligand to the complex is consistent with the increased π donor and chelation abilities, and explains the d–d absorption band that appears in the visible region (~643 nm) and the paramagnetic properties of the Cu(II) complex. Furthermore, Figure 11 depicts the orbital distribution patterns of phenylhydrazine, ligand L, and both Cu(II) complexes in the DMSO solvent model (CPCM) which retain the electronic characteristics obtained from calculations in vacuum. However, the use of DMSO provides a stronger dielectric stabilization effect on delocalized orbitals, especially on the LUMO and LUMO+1 orbitals. This can be seen from the more pronounced decrease in LUMO energy throughout the system when transferred to a polar medium. For example, in phenylhydrazine (Figure 11a) the LUMO decreases from -0.01 eV (vacuum) to -0.06 eV (DMSO), indicating that the π-interring orbital is more easily stabilized by polar solvents. This stabilizing effect is even stronger in the L

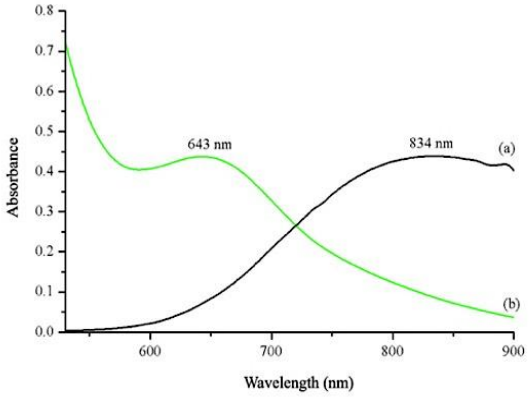


**Fig. 8:** UV-Vis spectra of $CuSO_4 \cdot 5H_2O$ (a) and Cu(II)-L (b) solution

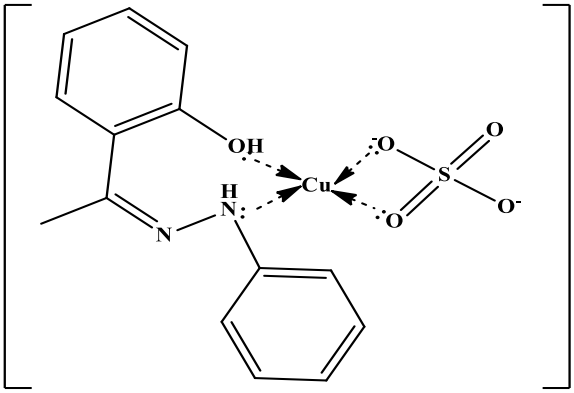


**Fig. 9:** Plausible structure of $[Cu(L)SO_4]$

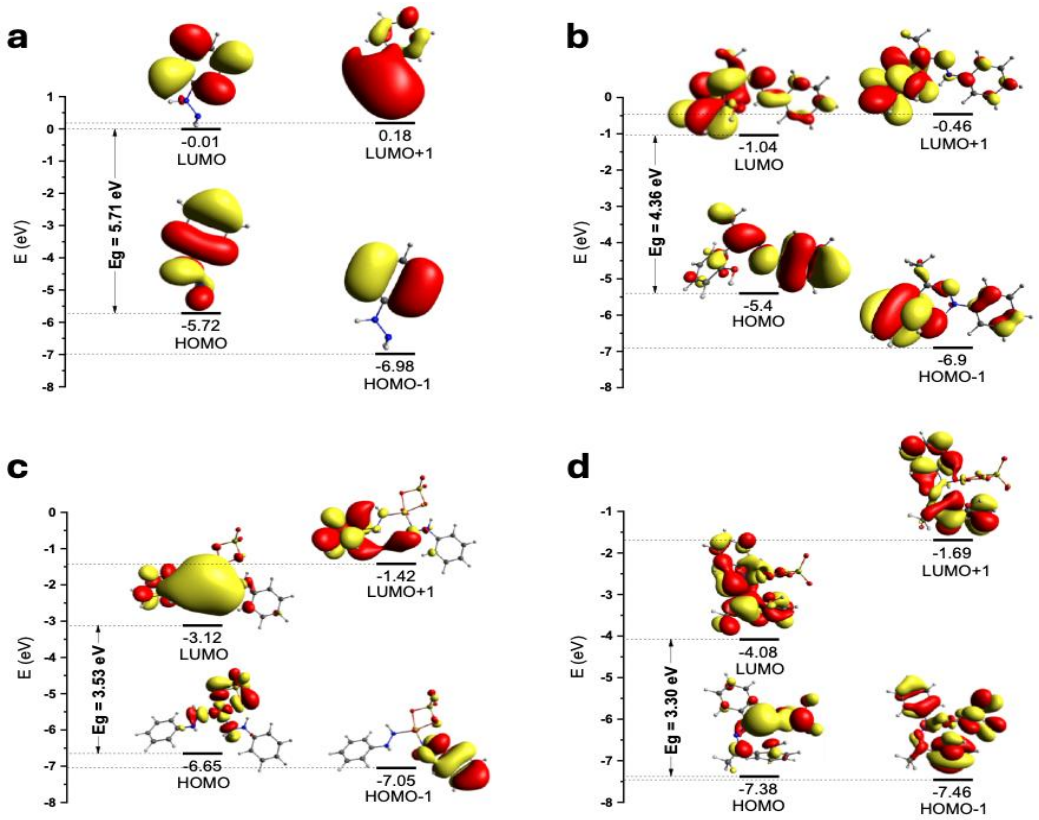


**Fig. 10:** Molecular orbital energy of (a) phenylhydrazine, (b) L, (c) Cu(phenylhydrazine)$_2$SO$_4$, and (d) Cu(L)SO$_4$ using TD-DFT on the PBE0-D4/def2 TZVPD(Cu,S,O,C)/def2-SVPD(H) level of theory in vacuum

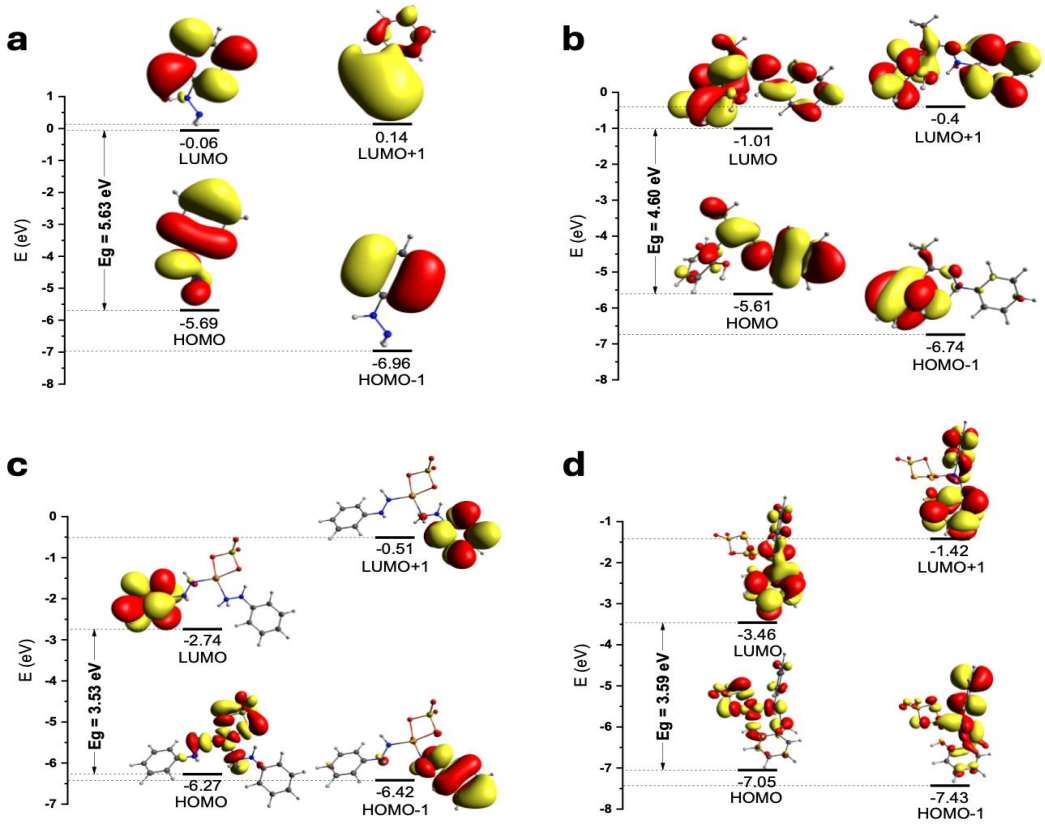


**Fig. 11:** Molecular orbital energy of (a) phenylhydrazine, (b) L, (c) [Cu(phenylhydrazine)$_2$SO$_4$] and (d) [Cu(L)SO$_4$] using TD-DFT on the PBE0-D4/def2-TZVPD(Cu,S,O,C)/def2-SVPD(H) level of theory in DMSO modelled using CPCM

ligand (Figure 11b), where the large π-conjugated system experiences a significant decrease in LUMO, resulting in a slight decrease in the band gap (from 4.36 eV in vacuum to 4.48 eV in DMSO), indicating competition between LUMO stabilization and a smaller HOMO readjustment. This small difference is consistent with the polar character of the C=N bond and the solvent-sensitive phenolate.

In the Cu(II) complex, the solvent effect becomes much more apparent. For Cu(phenylhydrazine)$_2$SO$_4$ (Figure 11c), the LUMO energy decreases again (-2.74 eV in DMSO compared to -3.12 eV in vacuum), but the HOMO also undergoes greater stabilization due to polar Cu-N interactions, resulting in a slightly larger band gap in the solvent. In contrast, in the [Cu(L)SO$_4$] complex (Figure 11d), the LUMO becomes lower (-3.46 eV) and the HOMO undergoes strong stabilization due to the increased polarity of the phenolate–azomethine donor, which now interacts with the solvent through the CPCM environment. This combination results in a band gap of 3.59 eV, slightly larger than that in vacuum (3.30 eV), indicating that the solvent medium enhances the LMCT/ILCT character and reduces the contribution of d–d transitions. Overall, the vacuum vs. DMSO differences consistently show that polar solvents stabilize ligand orbitals, especially at the LUMO level, while Cu(II) complexes undergo more complex energy adjustments due to metal-ligand contributions and electrostatic interactions.

Figure 12 shows a comparison of chemical reactivity parameters such as bandgap, ionization potential, electron affinity, chemical potential, chemical hardness, and electrophilic index for phenylhydrazine, ligand L, and two Cu(II) complexes, both under vacuum conditions and in DMSO solvent. In general, the formation of ligand L and then the Cu(II) complex causes a decrease in bandgap and significant changes in ionization potential and electron affinity, indicating an increase in the system's ability to undergo charge transfer. The Cu(L)SO$_4$ complex exhibits the highest electrophilicity and lowest chemical potential in both calculation conditions, confirming that this complex is the most reactive and most electronically stable species among all the compounds compared[36]. Additionally, the small differences between graphs Figures 12a and 12b indicate that polar solvents such as DMSO provide additional stabilization, particularly at low-energy orbitals, but do not alter the overall reactivity trends obtained from vacuum calculations.

### 3.4. Antibacterial Activity

Table 3 showing antibacterial inhibition zone diameters of CuSO$_4$·5H$_2$O, phenylhydrazine, L, Cu(II)-

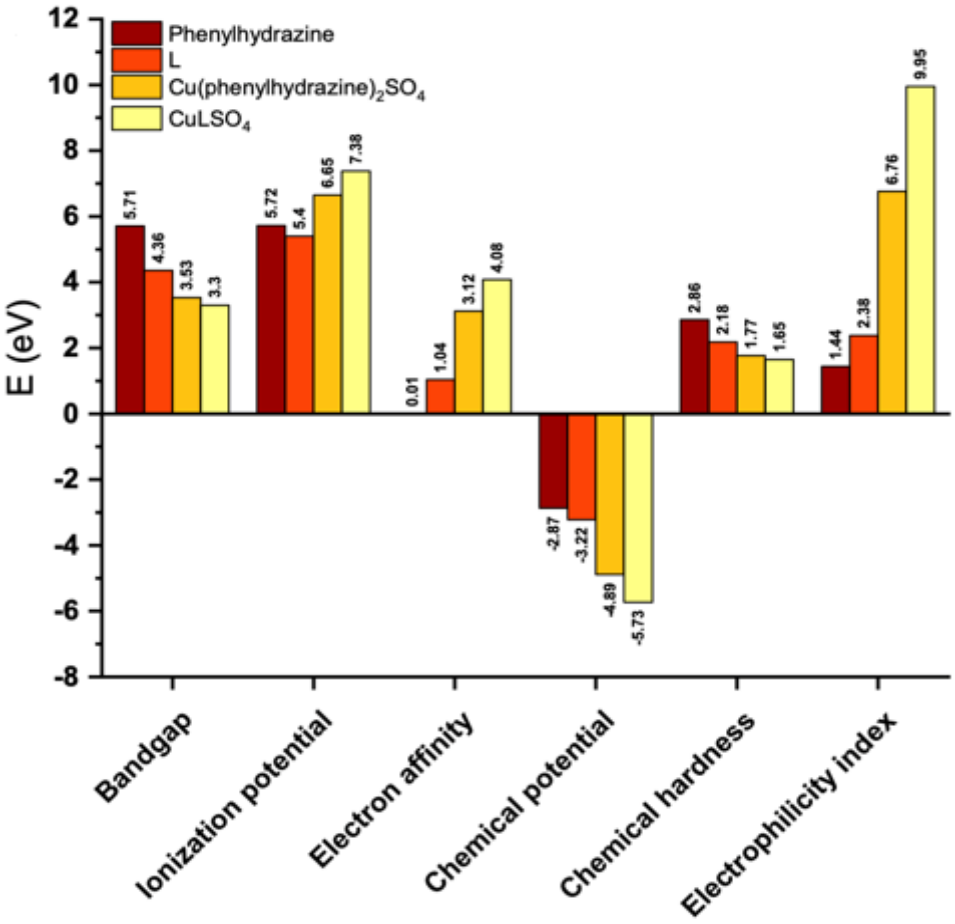


(a)

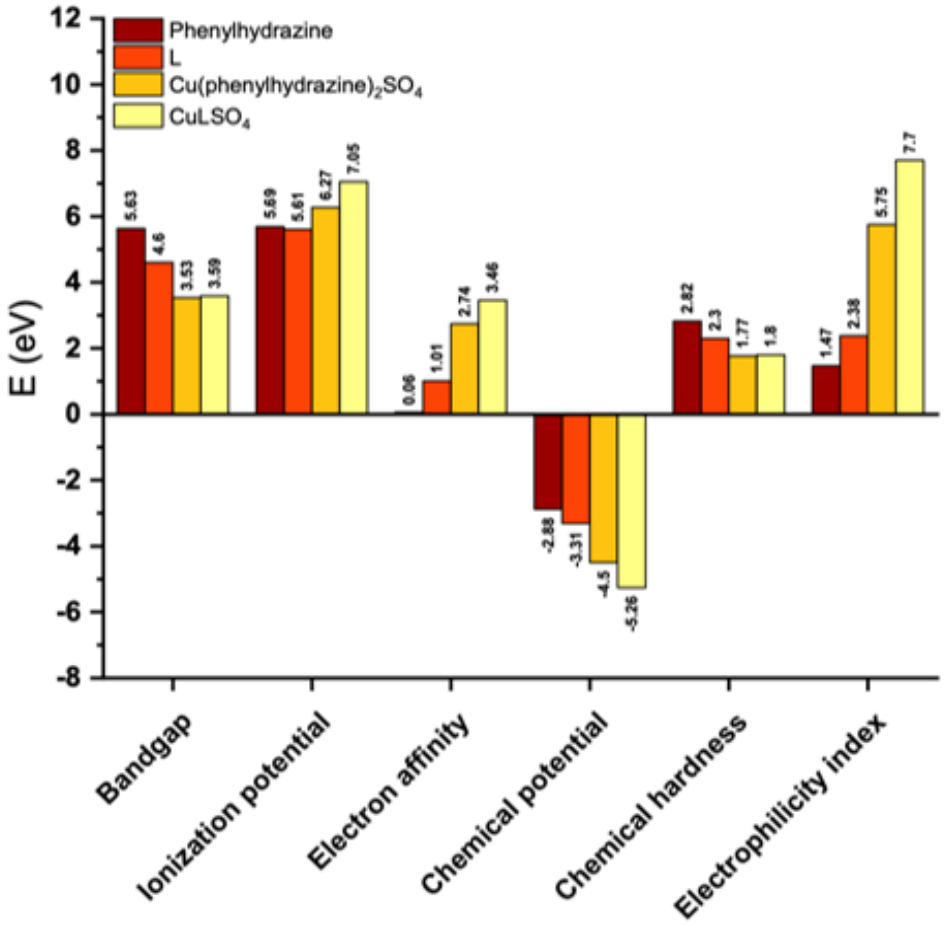


(b)

**Fig.12**: Global reactivity descriptors of phenylhydrazine, L, Cu(phenylhydrazine)$_2$SO$_4$, and CuLSO$_4$ in (a) vacuum and (b) DMSO

phenylhydrazine, and [Cu(L)SO$_4$], reveals that as the concentration increases, antibacterial effectiveness also increases. CuSO$_4$·5H$_2$O and phenylhydrazine ligands display the least inhibition at the highest tested concentrations. However, the antibacterial activity of phenylhydrazine improves significantly when it is modified into the Schiff base ligand, L, due to the addition of active groups NH, C=N, OH, and CH$_3$, compared to phenylhydrazine, which only has N-H and NH$_2$ groups[37]. Furthermore, the complexation of CuSO$_4$·5H$_2$O with phenylhydrazine and L demonstrates higher antibacterial efficacy than copper ion and the ligands. This enhancement is attributed to the complex's lipophilic nature, which facilitates easier penetration of bacterial cell walls or membranes[37]. This is because cationic metal ions themselves do not easily pass through bacterial cell membranes due to their hydrophilic character[38]. Based on the characteristics of complexes and ligands that can increase antibacterial activity, the synergy between the two can produce higher results. This is demonstrated by complexes with Schiff base ligands L, which have the highest inhibitory power compared to complexes with phenylhydrazine ligands against *S. aureus, S. epidermidis,* and *P. aeruginosa* bacteria. As reported by Radha et al. (2018), metal complexes with Schiff base ligands containing O and N donor atoms may inhibit enzyme production and increase bacterial cell death[39]. Additionally, complexes with bidentate ligands generally have higher antibacterial activity than those with monodentate ligands. Thus, the order of antibacterial activity from highest to lowest is [Cu(L)SO$_4$], Cu(II)-phenylhydrazine, L, phenylhydrazine, and CuSO$_4$·5H$_2$O, except *E. coli*, where Cu(II)-phenylhydrazine and [Cu(L)SO$_4$] complexes show similar antibacterial activity. It is also supporting computational data that ]Cu(L)SO$_4$] complex, which has the lowest bandgap, high electron affinity, and most negative chemical potential, shows the greatest tendency to interact with bacterial biomolecules through mechanisms such as membrane damage, enzyme inhibition, and ROS generation. The more extensive electron delocalization and LMCT/ILCT character of the Cu(II) complex also facilitates disruption of bacterial cell redox processes. Antibacterial activity against Gram-positive bacteria is generally higher than against Gram-negative bacteria. This is due to differences in the composition of the bacterial cell wall structure.

**Table 3:** Antibacterial inhibition zone diameters of $CuSO_4 \cdot 5H_2O$, phenylhydrazine, L, Cu(II)-phenylhydrazine and $[Cu(L)SO_4]$

| Compounds | Staphylococcus aureus ATCC 25923 Antibacterial activity (mm) Concentration (µg/disk) | | | | | Negative and Positive Control | |
|---|---|---|---|---|---|---|---|
| | 3.75 | 7.5 | 15 | 30 | 45 | DMSO (-) | Antibiotics (+)* |
| $CuSO_4 \cdot 5H_2O$ | - | 7.32 | 7.41 | 7.60 | 7.80 | - | 16.48 ± 0.38 |
| Phenylhydrazine | - | - | - | 6.99 | 8.93 | | |
| L | - | 7.57 | 8.44 | 9.53 | 9.86 | | |
| Cu(II)-Phenylhydrazine | - | 7.86 | 8.54 | 9.70 | 9.94 | | |
| $[Cu(L)SO_4]$ | - | 8.25 | 9.79 | 10.41 | 11.14 | | |
| **Staphylococcus epidermidis ATCC12228** | | | | | | | |
| $CuSO_4 \cdot 5H_2O$ | - | - | - | - | - | - | 24.76 ± 0.32 |
| Phenylhydrazine | - | 6.96 | 7.30 | 7.89 | 8.41 | | |
| L | - | 7.40 | 7.89 | 8.35 | 9.11 | | |
| Cu(II)-Phenylhydrazine | - | 7.77 | 8.89 | 9.36 | 9.86 | | |
| $[Cu(L)SO_4]$ | - | 7.84 | 9.64 | 13.21 | 15.39 | | |
| **Escherichia coli ATCC25922** | | | | | | | |
| $CuSO_4 \cdot 5H_2O$ | - | - | - | 6.83 | 6.87 | - | 28.39 ± 0.53 |
| Phenylhydrazine | - | - | - | - | - | | |
| L | - | - | 6.41 | 6.92 | 7.02 | | |
| Cu(II)-Phenylhydrazine | - | - | 6.61 | 7.17 | 7.45 | | |
| $[Cu(L)SO_4]$ | - | 6.61 | 6.90 | 7.24 | 7.69 | | |
| **Pseudomonas aeruginosa ATCC27853** | | | | | | | |
| $CuSO_4 \cdot 5H_2O$ | - | - | - | - | - | - | 20.08 ± 0.77 |
| Phenylhydrazine | - | - | - | - | - | | |
| L | - | - | 7.45 | 7.74 | 8.31 | | |
| Cu(II)-Phenylhydrazine | - | - | - | - | 6.78 | | |
| $[Cu(L)SO_4]$ | - | 9.47 | 105.3 | 13.03 | 13.96 | | |

Gram-positive bacteria have thicker cell walls compared to Gram-negative that are entirely composed of a layer of peptidoglycan[40]. This layer consists of a network of pores that allow foreign molecules such as antibacterial agents to enter the cell. Meanwhile, Gram-negative bacteria have a thin peptidoglycan layer covered by an outer membrane consisting of lipopolysaccharides, lipoproteins, and phospholipids. The presence of this outer membrane acts as a highly selective and effective permeability barrier, making it more difficult for antibacterial agents to penetrate. The antibacterial activity results of the metal ion, ligand, and Cu(II)-phenylhydrazine complex test compounds show that they are more effective at inhibiting Gram-negative bacteria than Gram-positive bacteria. However, the bacterial inhibition zone of the $[Cu(L)SO_4]$ complex is larger against *P. aeruginosa* (Gram-negative) than against *S. aureus* (Gram-positive). This indicates that the $[Cu(L)SO_4]$ complex has a broad spectrum against both Gram-positive and Gram-negative bacteria.

## 4. Conclusion

The hydrazone-derived Schiff base ligand (L) was successfully synthesized through a green and facile method by reacting phenylhydrazine with *o*-hydroxyacetophenone in a 1:1 molar ratio under ambient conditions with 1 hour of stirring. The resulting Cu(II) complex, formulated as $[Cu(L)SO_4]$, exhibited a planar rectangular geometry and was characterized as a non-electrolyte and paramagnetic compound. Its UV–Vis spectrum showed a single absorption band at 643 nm, confirming the complex formation. Modification of phenylhydrazine into ligand L effectively enhanced its antibacterial activity, which was further improved upon complexation with Cu(II). The $[Cu(L)SO_4]$ complex demonstrated stronger antibacterial activity than $CuSO_4 \cdot 5H_2O$, phenylhydrazine, L, and Cu(II)–phenylhydrazine complexes against *S. aureus*, *S. epidermidis*, and *P. aeruginosa*. However, its activity

against *E. coli* did not surpass that of the Cu(II)–phenylhydrazine complex.

## Acknowledgement

Sentot Budi Rahardjo expresses gratitude to Sebelas Maret University for the financial assistance through the PKGR-UNS grant scheme contract number: 462/UN27.22/PT.01.03/2026.

## References

1) C.E. Satheesh, P. Raghavendra Kumar, N. Shivakumar, K. Lingaraju, P. Murali Krishna, H. Rajanaika, and A. Hosamani, "Synthesis, structural characterization, antimicrobial and dna binding studies of homoleptic zinc and copper complexes of no schiff bases derived from homoveratrylamine," Inorganica Chim Acta, **495** 118929 (2019). doi:10.1016/J.ICA.2019.05.028.
2) S. Rostamizadeh, Z. Daneshfar, and H. Moghimi, "Synthesis of sulfamethoxazole and sulfabenzamide metal complexes; evaluation of their antibacterial activity," Eur J Med Chem, **171** 364–371 (2019). doi:10.1016/J.EJMECH.2019.03.002.
3) N. Terenti, A. Lazarescu, S. Shova, P. Bourosh, N. Nedelko, A. Ślawska-Waniewska, E. Zariciuc, and V. Lozan, "Synthesis, x-ray and antibacterial activity of new copper(ii) thiosemicarbazone complexes derived from 4-formyl-3-hydroxy-2-naphthoic acid," Inorganica Chim Acta, **571** 122216 (2024). doi:10.1016/J.ICA.2024.122216.
4) H.Q. Chang, L. Jia, J. Xu, T.F. Zhu, Z.Q. Xu, R.H. Chen, T.L. Ma, Y. Wang, and W.N. Wu, "Syntheses, crystal structures, anticancer activities of three reduce schiff base ligand based transition metal complexes," J Mol Struct, **1106** 366–372 (2016). doi:10.1016/J.MOLSTRUC.2015.11.001.
5) R. Malav, R.K. Sharma, and S. Ray, "Versatile applications of cobalt and copper complexes of biopolymeric schiff base ligands derived from chitosan," Int J Biol Macromol, **301** 140338 (2025). doi:10.1016/J.IJBIOMAC.2025.140338.
6) K.N. Prajapati, M.P. Brahmbhatt, J.J. Vora, P.B. Prajapati, and C. Author, "3d-transition metal chelates of schiff base ligand: synthesis, catalysis and antibacterial study," Int. J. ChemTech Res., **12** *(5)*, 56–63 (2019). doi:10.26479/2019.0502.56.
7) E.M. Zayed, A.M.M. Hindy, and G.G. Mohamed, "Molecular structure, molecular docking, thermal, spectroscopic and biological activity studies of bis‐schiff base ligand and its metal complexes," Appl Organomet Chem, **32** *(1)* (2018). doi:10.1002/aoc.3952.
8) G. Balakrishnaiah, J. Rangaswamy, and N. Naik, "ONE pot synthesis of piperidone based transition metal complexes and their antioxidant and antifungal activity studies," World Journal of Pharmaceutical Research, **8** (2019). doi:10.20959/wjpr20196-14860.
9) M.H. Khan, M. Cai, J. Deng, P. Yu, H. Liang, and F. Yang, "ROS-mediated multi-targeting anticancer mechanisms of copper (II) 2-hydroxy-1-naphthaldehyde complexes," Molecules, **24** *(14)* 2544 (2019). doi:10.3390/molecules24142544
10) A. Rauf, J. Ye, S. Zhang, L. Shi, M.A. Akram, and G. Ning, "Synthesis, structure and antibacterial activity of a copper(ii) coordination polymer based on thiophene-2,5-dicarboxylate ligand," Polyhedron, **166** 130–136 (2019). doi:10.1016/J.POLY.2019.03.039.
11) H.Z. Nejad, S.Y. Ebrahimipour, S.J. Fatemi, H. Ebrahimnejad, and J. Castro, "A novel dimeric copper(ii) complex derived from a schiff base ligand: structural insights and antibacterial potential," Polyhedron, **269** 117391 (2025). doi:10.1016/J.POLY.2025.117391.
12) Y.H. Li, D.X. Han, J.T. Liu, W.J. Li, D.N. An, M.H. Yao, M.Z. Ao, J.L. Wang, Y.J. Lv, X.Y. Xin, and Z.Q. Wang, "Two novel tetranuclear ni(ii)-based compounds constructed by polydentate schiff base ligands: structures, antibacterial activities and interaction with dna," Polyhedron, **279** 117660 (2025). doi:10.1016/J.POLY.2025.117660.
13) S. Kamali, and S. Amani, "Azo-imine based nickel(II), copper(II), and zinc(II) complexes: synthesis, physicochemical and spectral investigations, quantum chemical calculations, molecular docking studies, and antibacterial investigations," Inorganica Chim Acta, **563** 121904 (2024). doi:10.1016/J.ICA.2023.121904.
14) H.A. El-Boraey, and M.A. El-Salamony, "Transition metal complexes with polydentate ligand: synthesis, characterization, 3d molecular modelling, anticancer, antioxidant and antibacterial evaluation," J Inorg Organomet Polym Mater, **29** *(3)* 684–700 (2019). doi:10.1007/s10904-018-1042-1.
15) Shehnaz, W.A. Siddiqui, M.A. Raza, A. Ashraf, M. Ashfaq, M.N. Tahir, and S. Niaz, "Structure elucidation {single x-ray crystal diffraction studies, hirshfeld surface analysis, dft} and antibacterial studies of sulfonamide functionalized schiff base copper (II) and zinc (II) complexes," J Mol Struct, **1295** 136603 (2024). doi:10.1016/J.MOLSTRUC.2023.136603.
16) P.H.O. Santiago, M.B. Santiago, C.H.G. Martins, and C.C. Gatto, "Copper(ii) and zinc(ii) complexes with hydrazone: synthesis, crystal structure, hirshfeld surface and antibacterial activity," Inorganica Chim Acta, **508** 119632 (2020).

doi:10.1016/J.ICA.2020.119632.

17) A. Zülfikaroğlu, Ç. Yüksektepe Ataol, E. Çelikoğlu, U. Çelikoğlu, and Ö. İdil, "New cu(ii), co(iii) and ni(ii) metal complexes based on ono donor tridentate hydrazone: synthesis, structural characterization, and investigation of some biological properties," J Mol Struct, **1199** 127012 (2020). doi:10.1016/J.MOLSTRUC.2019.127012.
18) F.M. Elantabli, R.G. Mohamed, S.M. El-Medani, M. Haukka, R.M. Ramadan, and M.A. Afifi, "Structural investigations of new tridentate-phenylacetohydrazide schiff base metal chelates: x-ray diffraction, hirshfeld surface analyses, dft, antibacterial and molecular docking studies," J Mol Struct, **1299** 137230 (2024). doi:10.1016/J.MOLSTRUC.2023.137230.
19) K. Ghazal, S. Shoaib, M. Khan, S. Khan, M.K. Rauf, N. Khan, A. Badshah, M.N. Tahir, I. Ali, and A. ur Rehman, "Synthesis, characterization, x-ray diffraction study, in-vitro cytotoxicity, antibacterial and antifungal activities of nickel(ii) and copper(ii) complexes with acyl thiourea ligand," J Mol Struct, **1177** 124–130 (2019). doi:10.1016/J.MOLSTRUC.2018.09.028.
20) M. Bhushan, Y. Kumar, L. Periyasamy, and A.K. Viswanath, "Study of synthesis, structural, optical and magnetic characterizations of iron/copper oxide nanocomposites: a promising novel inorganic antibiotic," Materials Science and Engineering: C, **96** 66–76 (2019). doi:10.1016/J.MSEC.2018.11.009.
21) O.L. Cifuentes-Vaca, J. Andrades-Lagos, J. Campanini-Salinas, A. Laguna, D. Vásquez-Velásquez, and M. Concepción Gimeno, "Silver(i) and copper(i) complexes with a schiff base derived from 2-aminofluorene with promising antibacterial activity," Inorganica Chim Acta, **489** 275–279 (2019). doi:10.1016/J.ICA.2019.02.033.
22) A. Leite, L.J. Bessa, A.M.G. Silva, P. Gameiro, B. de Castro, and M. Rangel, "Antibacterial activity of naphthyl derived bis-(3-hydroxy-4-pyridinonate) copper(II) complexes against multidrug-resistant bacteria," J Inorg Biochem, **197** 110704 (2019). doi:10.1016/J.JINORGBIO.2019.110704.
23) Y.A. Rasyda, S.B. Rahardjo, and S.D. Marliyana, "Synthesis and structure characterization of copper(ii) complex with phenylhydrazine," J Phys Conf Ser, 1912 (1) 012029 (2021). doi:10.1088/1742-6596/1912/1/012029.
24) L.-H. Wang, X.-Y. Qiu, and S.-J. Liu, "Synthesis, characterization and crystal structures of copper(ii), zinc(ii) and vanadium(v) complexes, derived from 3-methyl- n ′ -(1-(pyridin-2-yl)ethylidene)benzohydrazide, with antibacterial activity," J Coord Chem, 72 (5–7) 962–971 (2019). doi:10.1080/00958972.2019.1590561.
25) V. Ordonez, H. Baykara, A. Riofrio, M. Cornejo, and R. Rodríguez, "Preparation and Characterization of Ecuadorian Bamboo Fiber-Low-Density Polyethylene (LDPE) Biocomposites," EVERGREEN Joint Journal of Novel Carbon Resource Sciences & Green Asia Strategy, 10 *(1)* 43–54 (2023). doi: 10.5109/6781037.
26) S. Kaushik, A. Kumar Verma, S. Singh, N. Kanojia, S. Panwar, S. Kindo, S. Uniyal, S. Goswami, D. Som, and N. Kumar Yadav, "Comparative Analysis of Fluid Flow Attributes in Rectangular Shape Micro Channel having External Rectangular Inserts with Hybrid Al 2 O 3 +ZnO+H 2 O Nano Fluid and (H 2 O) Base Fluid," EVERGREEN Joint Journal of Novel Carbon Resource Sciences & Green Asia Strategy, **10** *(2)* 851-862 (2023). doi: 10.5109/6792839
27) I. Sukirna, D. Dhaneswara, D.J. Siregar, J.F. Fatriansyah, N. Sofyan, A.H. Yuwono, and R. Muslih, "Synthesis of Mesoporous Silica from Sugarcane Bagasse Ash Using Pluronic 123 as a Colorant Adsorbent for Brilliant Green," EVERGREEN Joint Journal of Novel Carbon Resource Sciences & Green Asia Strategy, **11** *(2)* 1366–1374 (2024). doi: 10.5109/7183448
28) S. Yudha, C. Banon, R. Pertiwi, D.A. Triawan, and J.I. Han, "Cost-effective Synthesis of CeO 2-SiO 2 Based on Oil Palm Leaves for the Removal of Toxic Compounds," EVERGREEN Joint Journal of Novel Carbon Resource Sciences & Green Asia Strategy, **10** *(3)* 1307–1312 (2023). doi: 10.5109/7151676
29) A.A. Shanty, K.G. Raghu, and P. V. Mohanan, "Synthesis, characterization: spectral and theoretical, molecular docking and in vitro studies of copper complexes with hiv rt enzyme," J Mol Struct, 1197 154–163 (2019). doi:10.1016/J.MOLSTRUC.2019.06.097.
30) H. Syaima, S.B. Rahardjo, and V. Suryanti, "Facile and rapid synthesis of tetrakis-2-amino-5-methylpyridinecopper(ii) chloride pentahydrate," IOP Conf Ser Mater Sci Eng, **858** *(1)* 012019 (2020). doi:10.1088/1757-899X/858/1/012019.
31) N. Jyothi, N. Ganji, S. Daravath, and Shivaraj, "Mononuclear cobalt(II), nickel(II) and copper(II) complexes: synthesis, spectral characterization and interaction study with nucleotide by in vitro biochemical analysis," J Mol Struct, **1207** 127799 (2020). doi:10.1016/J.MOLSTRUC.2020.127799.
32) U.P. Ashok, S.P. Kollur, N. Anil, B.P. Arun, S.N. Jadhav, S. Sarsamkar, V.B. Helavi, A. Srinivasan, S. Kaulage, R. Veerapur, S. Al-Rashed, A. Syed, J. Ortega-Castro, J. Frau, N. Flores-Holguín, and D. Glossman-Mitnik, "Preparation, spectroscopic characterization, theoretical investigations, and in

vitro anticancer activity of Cd(II), Ni(II), Zn(II), and Cu(II) complexes of 4(3h)-quinazolinone-derived schiff base," Molecules, **25** *(24)* 5973 (2020). doi:10.3390/molecules25245973.

33) O.M.I. Adly, A. Taha, and S.A. Fahmy, "Synthesis, characterization of binary and ternary copper(ii)-semicarbazone complexes: solvatochromic shift, dipole moments and td-dft calculations," J Mol Struct, **1186** 362–376 (2019). doi:10.1016/J.MOLSTRUC.2019.02.103.
34) M. Shebl, A.A. Saleh, S.M.E. Khalil, M. Dawy, and A.A.M. Ali, "Synthesis, spectral, magnetic, dft calculations, antimicrobial studies and phenoxazinone synthase biomimetic catalytic activity of new binary and ternary cu(ii), ni(ii) and co(ii) complexes of a tridentate ono hydrazone ligand," Inorganic and Nano-Metal Chemistry, **51** *(2)* 195–209 (2021). doi:10.1080/24701556.2020.1770794.
35) S. Shaaban, Y.S. Al-Faiyz, G.M. Alsulaim, M. Alaasar, N. Amri, H. Ba-Ghazal, A.A. Al-Karmalawy, and A. Abdou, "Synthesis of new organoselenium-based succinanilic and maleanilic derivatives and in silico studies as possible sars-cov-2 main protease inhibitors," Inorganics (Basel), **11** *(8)* 321 (2023). doi:10.3390/inorganics11080321.
36) A.A. El-Saady, M.A. Ibrahim, M.M. El-Nahass, O.M. I Adly, A.A. M Farag, and N. Salah, "Exploring a novel copper(II) semicarbazone-pyranoquinoline complex: synthesis, spectroscopic profiling, and dft insights," Sci Rep **15**, 26205 (2025). doi: 10.1038/s41598-025-26205-8
37) M.A. El-Mogazy, A.Z. El-Sonbati, M.A. Diab, M.M. El-Zahed, H.M. Salama, E. Negm, S.G. Nozha, and S.M. Morgan, "Synthesis, spectroscopic, thermal, dna binding, antibacterial, antifungal and molecular docking studies: antipyrine hydrazone ligand and its transition metal complexes," J Mol Liq, **409** 125543 (2024). doi:10.1016/J.MOLLIQ.2024.125543.
38) L. Viganor, O. Howe, P. McCarron, M. McCann, and M. Devereux, "The antibacterial activity of metal complexes containing 1,10- phenanthroline: potential as alternative therapeutics in the era of antibiotic resistance," Curr Top Med Chem, **17** *(11)* 1280–1302 (2017). doi:10.2174/1568026616666161003143333.
39) V.P. Radha, S. Jone Kirubavathy, and S. Chitra, "Synthesis, characterization and biological investigations of novel schiff base ligands containing imidazoline moiety and their co(ii) and cu(ii) complexes," J Mol Struct, **1165** 246–258 (2018). doi:10.1016/J.MOLSTRUC.2018.03.109.
40) J.N.A. Tetteh, F. Matthäus, and E.A. Hernandez-Vargas, "A survey of within-host and between-hosts modelling for antibiotic resistance," Biosystems, **196** 104182 (2020). doi:10.1016/J.BIOSYSTEMS.2020.104182.